Research Article

SOHAG JOURNAL OF SCIENCES

https://doi.org/10.21608/sjsci.2024.275618.1186

The Nuclear Symmetry Energy Determination Using Chiral Forces and its Effects on Neutron Stars Properties

Ahmed Refaat, Mohamed A. El-Zohry, Ahmed Youssef and Khaled S. A. Hassaneen*

Physics Department, Faculty of Science, Sohag University, Sohag 82524, Egypt.
**Email: khaled.hassaneen@science.sohag.edu.eg*

Received: 8th March 2024, **Revised:** 7th April 2024, **Accepted:** 22nd May 2024
Published online: 6th June 2024

Abstract: An essential component of the equation of state (EOS) of isospin asymmetric nuclear matter is nuclear symmetry energy. It influences the structure of neutron stars and finite nuclei. We perform qualitative investigations within chiral forces and do Brueckner-Hartree-Fock calculations for nuclear and neutron matter EOS in order to further our understanding of the influence of the symmetry energy on nuclear properties. We introduce N3LO, a nucleon-nucleon potential of chiral effective field theory, with various cutoff parameter values. The single particle potential's standard and continuous choices are both applied. To ensure the empirical saturation property, a phenomenological term based on chiral forces is introduced, modeling the three-body interaction. Both low and high values of the baryon density are specified in a generalized form for the equations of state. The Tolman-Oppenheimer-Volkov equations for comparable neutron stars are solved using these equations as input. The global parameters (masses, radii, and composition) of a neutron star are systematically studied using the obtained nuclear equations of state.
Keywords: BHF theory, EOS, Pauli operator, symmetry energy, chiral forces and neutron star properties.

1. Introduction

In nuclear physics and astrophysics, the equation of state (EOS) of nuclear matter is crucial [1,3]. Numerous techniques have been used to study the EOS [4]. Various methods have been employed to investigate both the momentum distribution of nucleons and short-range correlations in nuclear matter, including the Bruckner-Hartree-Fock (BHF) approach. The BHF approach, which has been developed and applied in several investigations, is one of the generally recognized methods for infinite nuclear matter. It is based on the solution of the two-nucleon equation in the nuclear medium, which produces the so-called G-matrix, an energy and density dependent effective interaction [5]. The single particle potential used in BHF approach calculations is crucial. While the continuous choice assumes the self-consistent BHF potential extends above Fermi level, the standard choice takes into account zero single particle energy [6]. The possibility employed in this work is N3LO, or next-to-next-to-next-to-leading order [7]. A very straightforward many-body method—the non-relativistic BHF method with a standard and continuous single particle spectrum utilizing N3LO potential—is used to get the EOS.Although the chiral N3LO potential is non-local, it cannot be adequately expressed as a function of distance alone; instead, we must utilize the relative momentum between the nucleons. This potential is a high precision phenomenological potential; chiral perturbation theory's fourth order contains a NN potential. Below 290 MeV lab energy, the accuracy of the NN data reproduction is similar to that of phenomenological high-precision potentials. For a NN potential to be dependable up to 290 MeV, the fourth order is required and sufficient because NN potentials of order three and lower are known to be quantitatively weak. One, two, and three-pion exchanges as well as a collection of contact interactions with zero, two, and four derivatives make up the chiral N3LO potential. When describing experimental data, the chiral N3LO potential turns out to be just as precise as the Argonne V18 potential [8]. Since the early days of nuclear physics, it has been known that the EOS of nuclear matter contains a symmetry energy term. However, due to the development of radioactive ion beam facilities, which have made it possible to study the structure and reactions of neutron-rich nuclei [9], where the symmetry energy plays a significant role, the experimental and theoretical study of the symmetry energy and its density dependence is becoming an interesting topic. In nuclear physics and astro-nuclear physics, figuring out the precise form of the density dependence of nuclear symmetry energy is a highly significant and fascinating topic. Numerous significant nuclear properties, including the ground-state nuclei's structure, the drip line nuclei's structure, the neutron skin of nuclear systems, the dynamics of heavy-ion reactions, the physics of giant collective excitations, and the physics of neutron stars, are all determined by it [10-14]. The experimental and theoretical determination of the symmetry energy is highly significant and valuable, since it has a profound effect on the parameters of neutron stars, particularly in relation to its density dependence [15, 16]. Since symmetry energy is not a quantity that can be measured directly, it must be indirectly retrieved experimentally from observables that are related to the symmetry energy. Thus, the accuracy of the model used to describe the experimental observables will determine how the symmetry energy is determined experimentally. The binding energy loss for the system transitioning from symmetric nuclear matter (SNM) to pure neutron matter (PNM) is

explained by the symmetry energy. Neutron star properties are closely related to the EOS of nuclear matter at densities orders of magnitude greater than that of normal atomic nuclei. Essential parameters of neutron stars, including their mass range, the mass-to-radius ratio, the crust's thickness, and the speed at which they cool over time, can be deduced from the EOS [17,18].The EOS is evaluated from multiple approaches, utilizing information from various research projects, as high-energy nuclear collisions, studies of the monopole resonance in finite nuclei and supernova and neutron star observations [19]. Supernova simulations indicate that an EOS that is too pliable to sustain certain observed neutron star masses is required [20]. On the other hand, studies of high-energy nuclear collisions suggest a stiffer EOS and appear abnormally big neutron star masses [21,22]. As such, it is difficult to draw firm conclusions on the EOS at high densities. Nonetheless, a suggestive agreement points to a rather rigid EOS, which is essential to maintain maximum neutron star masses in a measurable range of 1.4MΘ to 1.9 MΘ, where MΘ is the solar mass [22].After the significant theoretical calculations of neutron star properties carried out independently by Tolman [23] and Oppenheimer and Volkoff [24], a number of later publications in the scientific literature offered various theoretical predictions examining the complexities of the EOS. We have been investigating features of neutron stars, like the mass-radius relationship. Important requirements have been set by Baldo et al. [25] for a realistic EOS to be used in the investigation of neutron star properties. These requirements include maintaining nuclear incompressibility for SNM at saturation compatible with empirical values [26,28], faithfully representing the saturation point for SNM, guaranteeing a symmetry energy consistent with nuclear phenomenology and stability at high densities, and guaranteeing that the speed of sound stays slower than the speed of light across all relevant densities within neutron stars.The EOS of SNM and PNM have been taken into consideration in the current work's computations. Then computing the symmetry energy and incompressibility. The major goal of this work is to discuss how the properties of nuclear matter are affected when the momentum-space cut-off value is changed. We will examine neutron star properties including the mass-radius relationship and other proparities using data from this EOS.

2. The theoretical model

2.1 BHF and Three body force correction

The G-matrix is the basis of the BHF approach, which is defined by the Bethe- Goldstone equation as:

$$G(w) = V + V\frac{Q}{\omega - H_o + i\eta}G(w) \quad (1)$$

Where ω is the starting energy, η is a small number, Ho is the unperturbed energy of the intermediate states, V is the bare 2N potential and Q is the Pauli operator which projects out states with two nucleons above the Fermi level and its relation donates it:

$$Q(k,k') = (1 - \Theta_F(k))(1 - \Theta_F(k')) \quad (2)$$

Where ΘF is the occupation probability of a free Fermi gas with a Fermi momentum k < kF and ΘF (k) = 1 for k < kF and zero otherwise. According to BHF approach, we can calculate the total energy of nuclear matter by:

$$E/A = \sum_k \frac{\hbar^2 k^2}{2m} + \frac{1}{2}\sum_{k'<k_F} < kk'|G(e(k) + e(k'))|kk' > \quad (3)$$

where $|kk' >$ refers to the anti-symmetrization of the G-matrix elements. The single particle energy e(k) is the sum of the single particle potential U(k) and the kinetic energy T and given by:

$$e(k) = T + U(k) = \frac{\hbar^2 k^2}{2m} + U(k) \quad (4)$$

where the U(k) is given by the self-consistent equation as:

$$U(k) = \sum_{k'<k_F} < kk'|G(e(k) + e(k'))|kk' > \quad (5)$$

By assuming a quadratic dependence of the single particle energy on the nucleon momentum, e(k) can be written in the formula:

$$e(k) = \begin{cases} \frac{\hbar^2 k^2}{2m} + \Delta & k \le k_F \\ \frac{\hbar^2 k^2}{2m^*} & k > k_F \end{cases} \quad (6)$$

where m∗ is the nucleon effective mass and Δ is a constant gives the single particle energy at k = 0. In the present work, we will perform our calculations for SNM and PNM in six situations using the BHF approach framework. In three cases, the single-particle potential is continuously chosen at different values (Λ = 450, 500, and 550 MeV) using the angle average approximation of the Pauli operator; in the other three cases, the conventional method is applied at the same Λ values.

The nuclear incompressibility K around the saturation point by:

$$K = 9\rho^2 \frac{\partial^2 (E/A)(\rho)}{\partial \rho^2}|_{\rho=\rho_0} \quad (7)$$

where the empirical value is 220 ± 40MeV [28].

The EOS of SNM and PNM gives us information on the iso-spin effects [29], specifically on the symmetry energy Esym. We can define the symmetry energy as:

$$E_{sym}(\rho) = \frac{1}{2}\frac{\partial^2 (\frac{E}{A})(\rho,\alpha)}{\partial \alpha^2}|_{\rho=\rho_0} \quad (8)$$

The asymmetry parameter is expressed by:

$$\alpha = \frac{\rho_n - \rho_p}{\rho} \quad (9)$$

where ρp and ρn are proton and neutron densities in asymmetric nuclear matte, respectively and total density ρ equals $\rho_n + \rho_p$. According to Hassaneen and Gad's study [14, 30], the binding energy per nucleon E/A fulfills the simple α2 law as in the whole asymmetry range:

$$\alpha^2 E_{sym} = \frac{E}{A}(\rho,\alpha) - \frac{E}{A}(\rho,\alpha = 0) \quad (10)$$

Therefore, if we take α = 1, we can calculate the symmetry energy Esym as the difference between the binding energy of PNM $\frac{E}{A}(\rho,\alpha = 1)$ and that of SNM $\frac{E}{A}(\rho,\alpha = 0)$ as follows:

$$E_{sym} = \frac{E}{A}(\rho,\alpha = 1) - \frac{E}{A}(\rho,\alpha = 0) \quad (11)$$

The density dependance of the symmetry energy has a great effect of neutron stars properties, so determining its value is very important.

It is commonly known that the BHF technique is unable to accurately forecast the saturation properties of nuclear matter.

Specically, it has not been able to replicate both the saturation [31,33] Fermi momentum (kFsat =1.36 ± 0.05 fm-1) and the binding energy per nucleon (E/A = -16 ± 1 MeV) at the same time.

Carbone et al. [34] have studied SNM with chiral two- and three-nucleon forces in both the BHF and self-consistent Greens functions. They proposed corrections due to effects of chiral three-nucleon forces for the EOS of nuclear matter. These effects can be studied by the contact term and its contribution to the total energy, which is proportional to CE. In the Hartree-Fock approximation this is

$$(\frac{E_{C_E}}{A})_{Chiral} = -5.5C_E(\frac{\rho}{\rho_0})^2 \quad (12)$$

Anticipated outcomes suggest that negative values of the contact term strength CE [35] contribute to a more repulsive nature in the EOS for nuclear matter. The proximity of the saturation point to the empirical value aligns with CE falling within the interval -0.20 to -0.85, wherein CE represents the intensity of the contact term in the three-nucleon interaction [36,38].

Rather than using chiral three-body forces, this relation is employed to simulate three-body forces in the current study. Thus, the final EOS has the form to provide observed nuclear matter relations.

$$\frac{E}{A} = \left(\frac{E}{A}\right)^{BHF} + \left(\frac{E_{C_E}}{A}\right)_{Chiral} \quad (13)$$

2.2 Neutron star equations:

Neutron stars and their properties are very interesting physical systems, such as radii and masses as function of the central density, can be calculated from the EOS of the β-stable matter or PNM contained in them at zero temperature. The EOS is microscopically obtained. After that, we briefly outline the derivation of neutron-star properties from its EOS. Firstly, we will consider the constituents of the neutron star which are protons, neutrons, and electrons. The total energy of the system Etot can be calculated from the equation:

$$E_{tot} = \frac{E}{A}(\rho, x_p) + x_p m_p + x_n m_n + \frac{E_e}{A} \quad (14)$$

with respect to xp. In eq. (13), mp and mn are the rest masses of proton and neutron, $\frac{E_e}{A}$ is the contribution from electrons to the total energy Etot and $\frac{E}{A}(\rho, x_p)$ is the binding energy per nucleon of β-stable matter. $\frac{E_e}{A}$ can be approximated by its relativistic free-gas expression, so the electron energy per nucleon becomes [39,40]:

$$\frac{E_e}{A} = \hbar c \frac{(3\pi^2 x_p)^{4/3}}{4\pi^2} \rho^{1/3} \quad (15)$$

where from the charge neutrality condition xp = xe.

Proton fraction xp is [41]:

$$x_p \cong \frac{(4S(\rho))^3}{(\hbar c)^3(3\pi^2\rho)} \quad (16)$$

Using the Tolman-Oppenheimer-Volkov (TOV) equations for the enclosed mass m and the total pressure P [24,25]

$$\frac{dP}{dr} = -\frac{G[m(r) + 4\pi^3 P/c^2][\epsilon + P/c^2]}{r[r - 2Gm(r)/c^2]},$$
$$\frac{dm(r)}{dr} = 4\pi\epsilon r^2 \quad (17)$$

where m(r) is the gravitational mass inside r, G is the gravitational constant and P(r) is the pressure at radius r.

Total mass density ϵ and pressure P of stellar matter can be calculated using:

$$P = \rho^2 \frac{dE_{tot}}{d\rho} \quad (18)$$

$$\epsilon = \rho \frac{E_{tot}}{c^2}, \quad (19)$$

where c is the speed of light.

One can integrate outwards from the origin (r = 0) to the point r = R when the pressure becomes zero in order to solve the set of equations (17) for P(r) and M(r). R is defined as the star's coordinate radius at this point. This can be accomplished by using the starting pressure value at r = 0, or Pc = P(r = 0). The total and the radius R. The star's mass, M ≥ M(R), is dependent on the value of Pc. The energy density ϵ(r) (or the density mass ρ(r)) in terms of the pressure P(r) must also be known in order to do the integration. In the current work, this relationship—which is the EOS for neutron star matter—has been derived using our model in several kinds of scenarios.

3. Results and discussion

In this study, we adopted the N3LO potential in order to determine the equation of state for symmetric nuclear matter (Fig. 1, left panel) and pure neutron matter (Fig. 1, right panel) for different momentum-space cut-off values, specifically Λ = 450, 500, and 550 MeV, while considering density ρ. The computations utilized the typical and continuous choice of the single-particle potential, employing the angle average approximation. The momentum-space cut-offs are depicted by the black and red solid curves at 450 MeV for the continuous and conventional choices, the black and red dotted curves at 500 MeV for the continuous and conventional choices, and the black and red dashed curves at 550 MeV for the continuous and conventional choices. The solid points correspond to the calculated saturation points, whereas the square box represents the experimental saturation point. Fig. 1 shows that as density ρ increases, the binding energy per nucleon for SNM decreases. However, when Λ= 550 MeV is used, the EOS assumes its correct form; the binding energy per nucleon falls until it hits the saturation point and then rises as the density ρ increases. At various levels of the momentum-space cut-off, the curves representing the conventional choice are more repulsive than those representing the continuous one. The EOS becomes increasingly repulsive and saturated as the momentum-space cut-off value increases. The binding energy per nucleon only takes positive values in the situation of pure neutron matter, as shown by the right panel of Fig. (1) and increases quickly with increasing density. Especially at low densities, the choice of the angle average approximation has very little effect. Particularly at low densities, the variations in the momentum-space cut-off values are negligible. This is due to the absence of $3S1-{}^3D_1$ contribution for PNM which

is responsible for the bound state of the SNM. The saturation points for N3LO potential in each of the situations under consideration are reported in Table (1). To reach the right saturation point, we need to make changes to the model that is being employed, as the predicted saturation point at Λ = 550 MeV differs greatly from the empirical one. Additionally, we have determined the incompressibility K value at the saturation point using Eq. (7) at Λ =550 MeV. When choosing continuously, the K value falls within the experimental value range.The symmetry energy as a function of density, as determined by Eq. (11), is displayed in Fig. 2. At the 450 MeV momentum-space cut-off, the continuous choice and the conventional one are represented by the blue, solid, and dashed-dotted curves; at the 500 MeV momentum-space cut-off, they are represented by the black dotted and dashed-double-dotted curves; and at the 550 MeV momentum-space cut-off, they are represented by the red dashed and double-dashed-dotted curves. It rises as density does. At the same momentum-space cut-off, the curves representing the continuous option and the conventional choice are nearly similar. This is referring to the symmetry energy's weak dependency on the angle average approximation selection. There is no effect of altering the momentum-space cut-off value on the symmetry energy. Furthermore, as table (1) illustrates, the computed symmetry energy at the saturation point differs considerably from the empirical one. This suggests that we need to make adjustments to our model. We observed that the accurate saturation point for SNM is not reproduced by non-relativistic computations based on pure two-body interactions Usually, three-body forces or relativistic correction is introduced in order to correct this known deficiency. Gad used every order of NN effective field interaction to examine the EOS of nuclear and pure neutron matter in the frame of BHF in a recent work [42, 43]. He found that there were no saturation features in the final EOS that was only based on the BHF technique. Therefore, in order to obtain the saturation properties with an accurate picture, all calculations require relativistic corrections or three-body forces. To achieve the approved saturation qualities in the current work, we implement an adjustment caused by the simulated chrial three-body force, which is given by Eq. (12). Our calculations for the EOS, or the energy per particle E/A as a function of density ρ, after adding Chiral as 3BF (N3LO + 3BF) potential at various momentum-space cut-off values Λ = 450, 500, and 550 MeV, are shown and discussed. With the continuous selection of the single-particle potential and the conventional (standard) one, the calculations were performed using the angle average approximation. Plotting of the EOS computation results for SNM is shown in Fig. (3). At the 450 MeV momentum-space cut-off, the continuous choice and the conventional one are represented by the red stars and black circles, respectively; at the 500 MeV momentum-space cut-off, they are represented by the red (x sign) and black (square sign), respectively; and at the 550 MeV momentum-space cut-off, they are represented by the red (triangle-up sign) and the black (triangle-down sign), respectively. The green square box represents the empirical saturation point. This figure shows how EOS takes on its appropriate shape: the binding energy per nucleon for SNM reduces with increasing density ρ, but for EOS, it decreases until it reaches the saturation point and then increases. For continuous choice, the saturation point at ρ = 0.22 fm^{-3} was near the empirical value; however, for conventional choice, it was pushed to a higher density (0.27 fm^{-3} to 0.29 fm^{-3}).

Table 1: The saturation points as a function of density for N3LO potential at Λ= 550 MeV.

Model	ρ_0 (fm^{-3})	E/A (MeV)	K (MeV)	E_{sym} (MeV)
BHF (cont)	0.5713	-27.7360	262.1584	68.6487
BHF (conv)	0.5974	-25.4314	186.6210	68.0062
Empirical	0.17 [33]	-16 ± 1 [33]	220 ± 40[28]	31.7 ± 3.2[32]

Table 2: The saturation points as a function of density for N3LO+ 3BF potential at different Λ.

Model	ρ_0 (fm^{-3})	E/A (MeV)	K (MeV)	E_{sym} (MeV)
BHF+3BF (cont450)	0.22	-16.2573	226.2	37.25804
BHF+3BF (cont500)	0.22	-16.2492	214.3	38.07056
BHF+3BF (cont500)	0.22	-16.1456	207.3	34.66771
BHF+3BF (conv450)	0.29	-16.2116	239.2	41.75908
BHF+3BF (conv500)	0.275	-15.9306	213.4	41.49356
BHF+3BF (conv550)	0.27	-15.9022	206	39.87916
Empirical	0.17 [33]	-16 ± 1 [33]	220 ± 40[28]	31.7 ± 3.2[32]

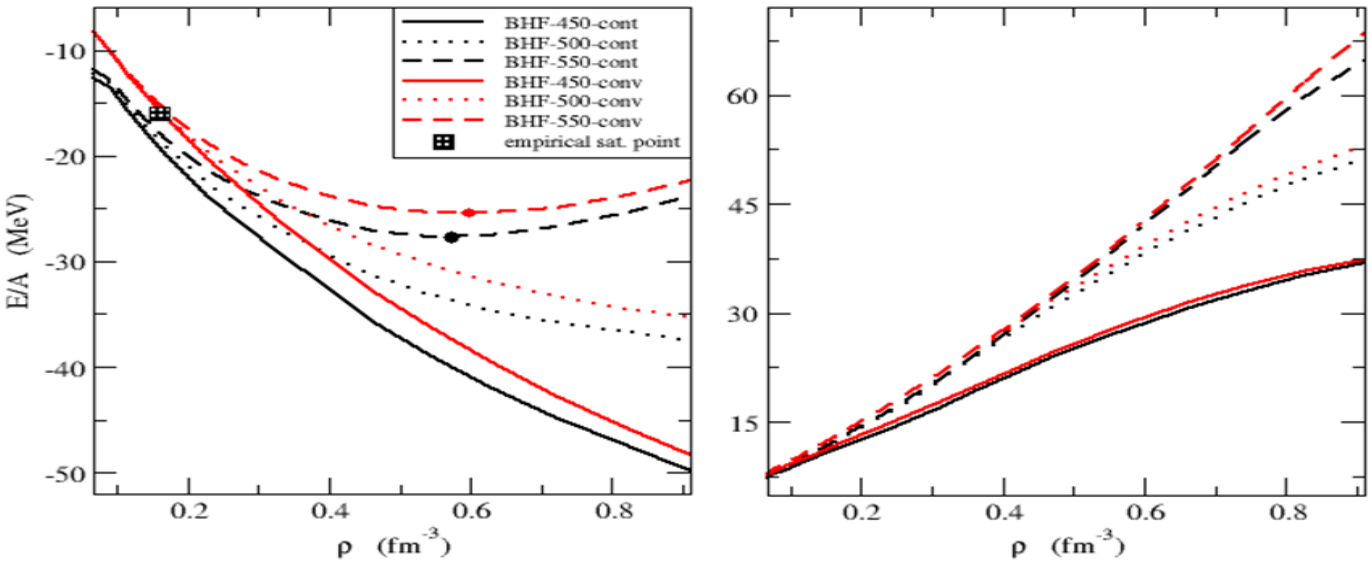

Fig. 1: binding energy per nucleon E/A as a function of density ρ using N3LO (left panel) symmetric nuclear matter (right panel) pure neutron matter at different values of Λ.

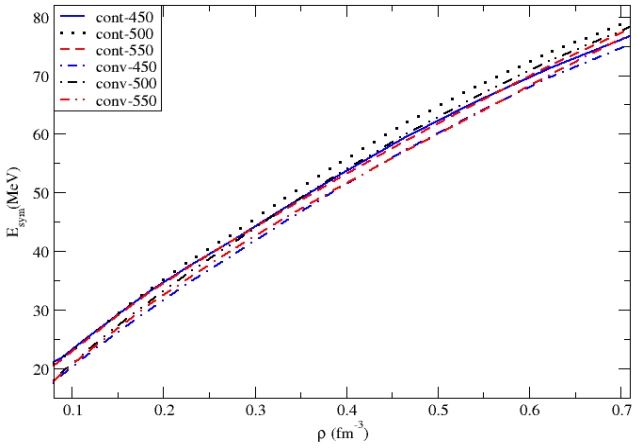

Fig. 2: The symmetry energy as a function of density ρ using N3LO potential at different values of Λ

At various levels of the momentum-space cut-off, the curves representing the continuous choice are more repulsive than those representing the conventional one. The EOS becomes increasingly repulsive and saturated as the momentum-space cut-off value decreases. The saturation point findings are shown in Table (2). The PNM EOS results are displayed in Fig. (4). With increasing density, the binding energy per nucleon only rises quickly to positive levels. Especially at low densities, the choice of the angle average approximation has very little effect. Particularly at low densities, the variations in the momentum-space cut-off values are negligible. This is because the PNM, which is in charge of the SNM's bound state, does not have a $^3S_1-^3D_1$ contribution. The symmetry energy as a function of density is displayed in Figure 5. Both the continuous and conventional choices are represented by the red solid and black dashed-dotted curves, respectively. At the 450 MeV momentum-space cut-off; the continuous and conventional choices are represented by the red dotted and black dashed-double-dotted curves, respectively. Further, at the 500 MeV momentum-space cut-off; and the continuous and conventional choices are represented by the red dashed and black double-dashed-dotted curves, respectively, at the 550 MeV momentum-space cut-off. The figure shows that as density rises, so does the symmetry energy. At the same momentum-space cut-off, the curves representing the continuous choice and the standard one are nearly similar. This is referring to the symmetry energy's weak dependency on the angle average approximation selection The effect of altering the momentum-

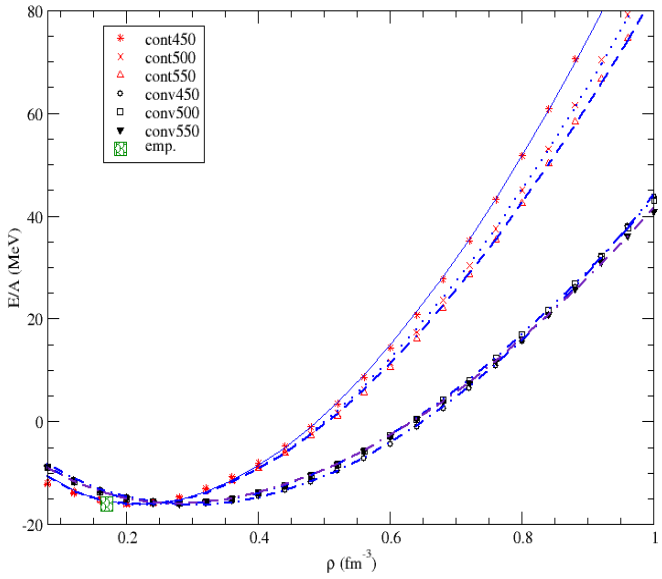

Fig. 3: The binding energy per nucleon E/A as a function of density ρ using N3LO+3BF for Symmetric nuclear matter.

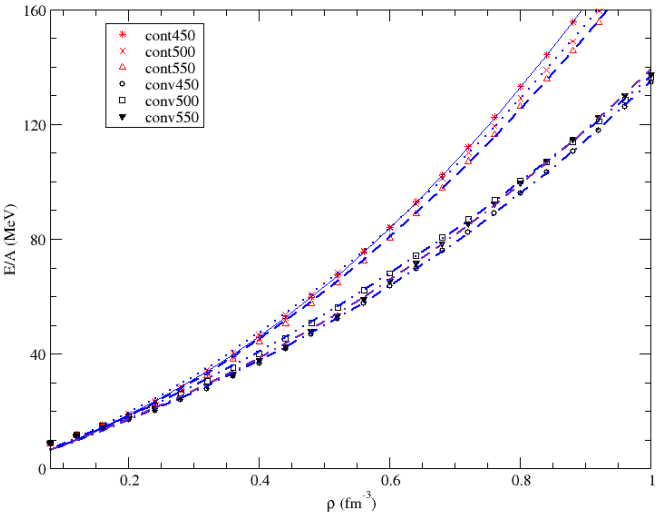

Fig. 4: The binding energy per nucleon E/A as a function of density ρ using N3LO+3BF for Pure neutron matter.

space cut-off value on the symmetry energy is negligible. Additionally, as table (2) shows, the computed symmetry energy at the saturation point is closer to the empirical one.

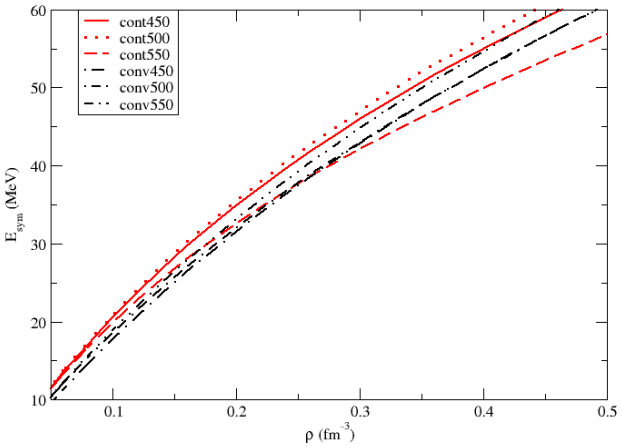

Fig. 5: The symmetry energy as a function of density ρ using N3LO + 3BF at different values of Λ.

2.2 Neutron star properties

The BHF approximation limited to two-nucleon correlations, overlooks certain correlation effects and exhibits breakdowns at both low and high densities [44, 45]. In addressing these challenges, Li and Schulze [46] introduced an appealing parametrization for the EOS. Their work demonstrates the effectiveness of a polynomial in accurately fitting a diverse array of nuclear EOSs at lower densities:

$$\frac{E}{A}(\rho) = a\,\rho + b\,\rho^{\gamma} \qquad (20)$$

The use of parameters a, b, and γ in the provided equation, with their corresponding numerical values reported in Table 3, exemplifies a fitting procedure undertaken within a specified density range. This procedure is essential for tailoring the EOS to accurately represent nuclear matter behavior within the given density limits. Importantly, the fitted EOS is then applied in the current study to extrapolate to higher densities, proving particularly advantageous for the analysis of neutron star observables. This extrapolation allows for a more comprehensive understanding of the EOS under extreme conditions, providing valuable insights into the properties of neutron stars.Since the muon contribution does not materially change the overall characteristics of the neutron stars, the current neutron star matter is made up of n, p, and e− instead of include the muon in the total EOS [47]. The only thing keeping the neutron star in hydrostatic equilibrium besides gravity is the pressure created by the compressed nuclear materials. Moreover, a lower central density and a greater maximum mass are supported by a stronger EOS. After solving the TOV general relativistic equations for a spherically symmetric (nonrotating) neutron star, the gravitational mass of the star MG is found as a function of the central density ρc and the stellar radius R.The dependence of the neutron star masses on the stellar radius R and the core density ρc is shown in Figures 6 and 7, respectively, for momentum-space cut-offs of 450, 500, and 550 MeV. The conventional choice is shown in the right panel, and the continuous option is represented in the left panel. The lines with black dash, red solid and blue dash dotted indicate the BHF+3BF at 450, 500, and 550 cut-offs, respectively. According to Figures 6 and 7 show us that the upper limit mass of a neutron star at a core density ρc=1.5 fm-3 and radius R of approximately 8.911 km is Mmax ≈ 1.85MΘ in the case of continuous 450 computations. Furthermore, for continuous 500, it is found that Mmax ≈ 1.76 MΘ at central density of ρc = 1.5 fm-3 with a radius R ≈ 8.931 km. For continuous 550, a maximum mass of star is Mmax ≈ 1.6 MΘ at central density of ρc =1.5 fm-3 with a radius R ≈ 8.551 km. In the case of conventional 450, Mmax of NS ≈ 1.84 MΘ at central density of ρc =1.5 fm-3 with a radius R ≈ 8.821 km. Further for conventional 500, Mmax ≈ 1.51 MΘ at a central density of ρc =1.5 fm-3 and a radius R ≈ 8.631 km were found. Finally, for a typical 550, Mmax of NS ≈ 1.597 MΘ at a central density of ρc =1.5 fm-3 and a radius R ≈ 8.591 km were found. Table 4 provides a summary of all the findings. The condition that EOS models for neutron star materials yield maximum stable masses of at least 2 MΘ has been confirmed by observations of big stars. Many of the softer theoretical EOS models were ruled out by observations of huge neutron stars because these models are known as "stiff," which means they have a large pressure for a given density. MSP J0740+6620, one of the heaviest millisecond pulsars recorded to far, with a measured mass of $2.14^{+0.10}_{-0.09}$ MΘ, is an example of such enormous observations [48]. Moreover, there have never been direct measurements of the radius of a neutron star, and estimating the radius by a variety of methods has significant uncertainty in comparison to accurate measurements of mass. The radius of a purely hadronic neutron star is bound to be 12.0km < R < 13.45km, according to recent calculations by Most et al. [49] using a new approach. . Abbott et al. [50] calculated the neutron star radius at 10.5 km < R < 13.3km at the same time. A new estimate of 8.9 km < R < 13.2 km for the common NS radius was obtained by De et al. [51]. This indicates that certain NS obsarvables are not well supported by the current model. We can replace the current model if we so want.

Table (3): Equation (20) is used to fit the parameters of the EOS for SNM and PNM with BHF + (chiral 3BF) model.

	Cut-off	A	b	γ
SNM continuous	450+ 3BF	-208.922	307.218	1.5430
	500+ 3BF	-232.953	320.659	1.4629
	550+ 3BF	-246.728	329.479	1.4242
PNM continuous	450+ 3BF	77.035	117.071	2.2213
	500+ 3BF	76.762	106.025	2.0260
	550+ 3BF	70.564	108.171	2.3682
SNM conventional	450+ 3BF	-138.585	182.583	1.6400
	500+ 3BF	-173.713	217.098	1.4872
	550+ 3BF	-188.427	229.919	1.4383
PNM conventional	450+ 3BF	77.864	57.243	2.3910
	500+ 3BF	81.056	55.566	2.0738
	550+ 3BF	77.476	61.541	2.2926

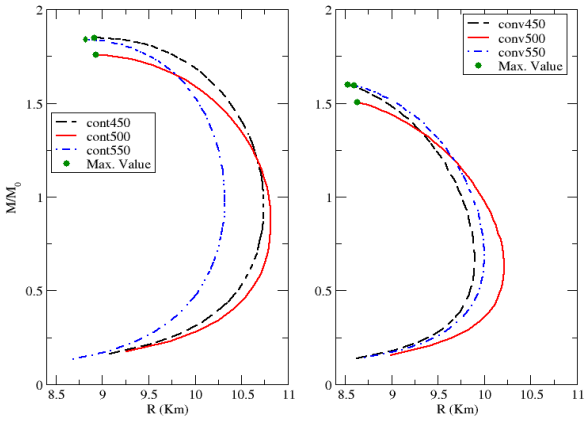

Fig. 6: Neutron star gravitational masses plotted as a function of the stellar radius**.**

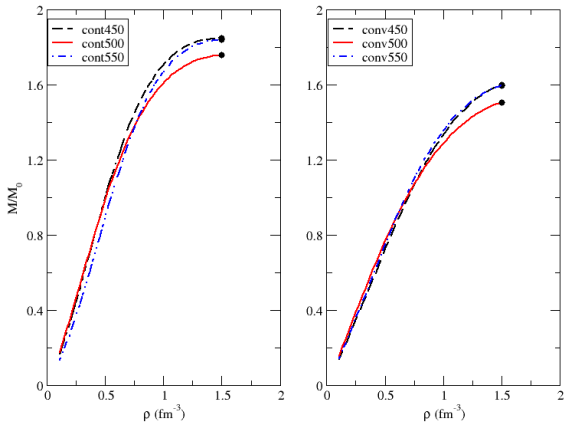

Fig. 7: Neutron star gravitational masses as a function of the central density ρ.

Table (4): The max value of radius R, central density ρ_c, and mass M_{max} of the neutron star.

	Cut-off	M_{max} ***(Mʘ)***	R (Km)	ρ_c (fm^{-3})
continuous	450+ chiral	1.85	8.911	1.5
	500+ chiral	1.76	8931	1.5
	550+ chiral	1.84	8.821	1.5
conventional	450+ chiral	1.6	8.551	1.5
	500+ chiral	1.51	8.631	1.5
	550+ chiral	1.597	8.591	1.5

4. Conclusion

We conclude this analysis by pointing out that the EOS is extremely sensitive to any change in the momentum-space cutoff, particularly at high densities. It was discovered that the EOS of SNM exhibits a greater momentum-space cut-off dependence as compared to that of PNM. When employing the angle average approximation with his two options, increasing the momentum-space cut-off number has an improvement; EOS takes on its correct shape and saturates at Λ = 550 MeV.This complements the earlier research, however the impacts of this augmentation are not particularly strong near the empirical saturation point. Future studies will investigate a correction to the proposed model that takes this difficulty into account, including three-body force and Dirac contributions corrections. The correct binding energy per nucleon and the symmetry energy values at the saturation are still missing. The TOV equation of general relativity, which yields the mass and radius of neutron stars, can be numerically solved using the current EOSs of nuclear and pure neutron matter. It turns out that the stiffness of the proposed EOS has a critical role in determining both maximum stable masses and radii. An additional significant outcome is that NS parameters, including radius and total mass, are calculable using microscopic models. Additionally, the results of the non-relativistic EOS calculation may appear softer, and a uniform EOS calculation is required to fully characterize the features of the neutron star and its structure [52,54].

CRediT authorship contribution statement:

Conceptualization, Khaled S. A. Hassaneen. and Ahmed Refaat; methodology, Khaled S. A. Hassaneen; software, Khaled S. A. Hassaneen; validation, Khaled S. A. Hassaneen, Mohamed A. El-Zohry and Ahmed Youssef; formal analysis, Khaled S. A. Hassaneen, Ahmed Youssef and Ahmed Refaat; investigation, Khaled S. A. Hassaneen, Mohamed A. El-Zohry and Ahmed Refaat; resources, Khaled S. A. Hassaneen; data curation, Khaled S. A. Hassaneen, Ahmed Youssef and Ahmed Refaat; writing—original draft preparation, Ahmed Refaat; writing—review and editing, Khaled S. A. Hassaneen and Ahmed Refaat; visualization, Khaled S. A. Hassaneen, Mohamed A. El-Zohry and Ahmed Youssef; supervision, Khaled S. A. Hassaneen, Mohamed A. El-Zohry, and Ahmed Youssef; project administration, Khaled S. A. Hassaneen, Mohamed A. El-Zohry, and Ahmed Youssef; funding acquisition, Khaled S. A. Hassaneen. All authors have read and agreed to the published version of the manuscript.

Data availability statement

The data used to support the findings of this study are available from the corresponding author upon request.

Declaration of competing interest

The authors declare that they have no known competing financial interests or personal relationships that could have appeared to influence the work reported in this paper.

References

[1] J. Margueron, E. van Dalen, C. Fuchs, *Phys. Rev. C*, 76(2007) 034309.
[2] K. S. A. Hassaneen, H. Müther, *Phys. Rev. C*, 70(2004) 054308.
[3] H. Mansour, K. Gad, K. S. A. Hassaneen, *Prog. Theor. Phys*, 123 (2010) 687-700.
[4] H. Müther and A. Polls, *Progress in Particle and Nuclear Physics*, 45 (2000) 243 – 334.
[5] K. S.A. Hassaneen, Eur. *Phys. J. Plus*, 133 (2018) 484.
[6] H. Kümmel, K.H. Lührmann, and J.G. Zabolitzky, *Physics Reports*, 36 (1978) 1 – 63.
[7] D. R. Entem, R. Machleidt and Y. Nosyk, *Phys. Rev. C*,96 (2017) 024004.
[8] I. Tanihata., J. Phys. G: Nucl. *Part. Phys*., 22 (1996) 157.
[9] N. van Giai, B. V. Carlson, Z. Ma and H. Wolter, *J. Phys. G: Nucl. Part. Phys*., 37(2010) 064043.
[10] E. N. E. van Dalen and H. Müther, *Int. J. Mod. Phys*., 19 (2010) 2077.
[11] B.A. Li, L.W. Chen and C. M. Ko, *Phys. Rep*., 464 (2008) 113.
[12] V. Rodin, *Prog. Part. Nucl. Phys*, 59 (2007) 268.
[13] K.S.A. Hassaneen, *Phys. Res. Int*, 2013(2013) 415605.
[14] K.S.A. Hassaneen and K. Gad, *J. Phys. Soc. Jpn*, 77(2008) 084201.
[15] Ø. Elgarøy, L. Engvik, M. Hjorth-Jensen and E. Osnes, *Phys. Rev. Lett*, 77 (1996) 1428.
[16] F. Weber, N.K. Glendenning, M.K. Weigel, *Astrophys. J*, 373 (1991) 579.
[17] Khaled S.A. Hassaneen, Eur. *Phys. J. A*, 53 (2017) 9.
[18] H. M. Abou-Elsebaa, E. M. Darwish, and Kh. S. A. Hassaneen, *Moscow Univ. Phys*, 75 (2020) 320–330.
[19] G. Bao, L. Engvik, M. Hjorth-Jensen, E. Osnes and E. Østgaard, *Nucl. Phys. A*, 575 (1994) 707.
[20] A.W. Steiner, M. Hempel and T. Fischer, *Astrophys. J*, 774 (2013) 17.
[21] T. Fischer, M. Hempel, I. Sagert, Y. Suwa and J. Schaffner-Bielich, *Eur. Phys. J. A*, 50 (2014) 46.
[22] S.E. Thorsett, Z. Arzoumanian, M. M. McKinnon and J.H. Taylor, *Astrophys. J*, 405 (1993) 29.
[23] J. Oppenheimer and G. Volkoff, *Phys. Rev*., 55 (1939) 374-381.
[24] R.C. Tolman, *Proc. Natl. Acad. Sci. U.S.A*, 20 (1934) 169–176.
[25] M. Baldo, I. Bombaci and G.F. Burgio, *Astron. Astrophys*, 328 (1997) 274.
[26] E. Khan, and J. Margueron, *Phys. Rev. C*, 88:034319 (2013).
[27] J.R. Stone, N.J. Stone and S.A. Moszkowski, *Phys. Rev. C* ,89 (2014) 044316.
[28] Wang et al., *Physics Letters B*, 778 (2018) 207–212.
[29] N. B. Zhang, B.A. Li, and J. Xu, *ApJ*, 859 (2018) 90.
[30] Kh. Gad, and Kh. Hassaneen, *Nuclear Physics A*, 793 (2007) 67–78.
[31] Kh. S. A. Hassaneen, H. M. Abo-Elsebaa, E. A. Sultan and H. M. M. Mansour, *Annals of Physics*, 326 (2011) 566.
[32] H. Mansour and K. S. A. Hassaneen, *Phys. At. Nucl*, 77 (2014) 290.
[33] B. D. Day, *Rev. Mod. Phys*, 39 (1967) 719.
[34] A. Carbone, A. Rios, and A. Polls, *Phys. Rev. C*, 88(2013) 044302.
[35] A. Ekström, G. Baardsen, C. Forssén, G. Hagen, M. Hjorth-Jensen, G. R. Jansen, R. Machleidt, W. Nazarewicz, T. Papenbrock, J. Sarich, and S. M. Wild, *Phys. Rev. Lett*, 110 (2013) 192502.
[36] A. Nogga, P. Navrátil, B. R. Barrett, and J. P. Vary, *Phys. Rev. C*, 73 (2006) 064002.
[37] P. Navrátil, V. G. Gueorguiev, J. P. Vary, W. E. Ormand, and A. Nogga, *Phys. Rev. Lett*., 99 (2007) 042501.
[38] D. Gazit, S. Quaglioni, and P. Navrátil, *Phys. Rev. Lett*,103 (2009) 102502.
[39] I. Bombaci and U. Lombardo, *Phys. Rev. C*, 44 (1991) 1892.
[40] P.G. Krastev and F. Sammarruca, *Phys. Rev. C*, 74(2006) 025808.
[41] M. Baldo and G.F. Burgio, *Prog. Part. Nucl. Phys*, 91 (2016) 203-258.
[42] Kh. Gad, *Indian J Phys*, 95 (2021) 1499–1508.
[43] Kh. Gad, *Pramana – J. Phys*, 95 (2021) 108.
[44] X. Wu, H. Müther, M. Soffel, H. Herold and H. Ruder, *Astron. Astrophys*, 246 (1991) 411.
[45] F. Hofmann, C.M. Keil and H. Lenske, Phys. Rev. C, 64, 025804 (2001).
[46] Z.H. Li and H.J. Schulze, *Phys. Rev. C*, 78(2008) 028801.
[47] Ch.C. Moustakidis, *Phys. Rev. C*, 91(2015)035804.
[48] H.T. Cromartie, et al., *Nature Astronomy*, 4 (2020) 72–76.
[49] E. R. Most, L. R. Weih, L. Rezzolla, and J. Schaffner-Bielich, *Phys. Rev. L*, 120(2018) 261103.
[50] B. P. Abbott, R. Abbott, T. D. Abbott, et al., *Phy. Rev. L*, 121 (2018) 161101.
[51] S. De, D. Finstad, J. M. Lattimer, D. A. Brown, E. Berger, and C. M. Biwer, *Phys. Rev. Lett*., 121 (2018) 091102.
[52] F. Sammarruca, *Symmetry*, 15 (2023) 450.
[53] F. Sammarruca, R Millerson, *Universe*, 8 (2022) 133.
[54] D Logoteta and I Bombaci, *Publications of the Astronomical Society of Australia*, 35 (2018) 1–9.